Zika virus directly infects peripheral neurons and induces cell death

Yohan Oh[1,2], Feiran Zhang[3], Yaqing Wang[4], Emily M Lee[5], In Young Choi[1], Hotae Lim[1], Fahimeh Mirakhori[1], Ronghua Li[3], Luoxiu Huang[3], Tianlei Xu[6], Hao Wu[7], Cui Li[4], Cheng-Feng Qin[8], Zhexing Wen[1,9,10], Qing-Feng Wu[4], Hengli Tang[5,17], Zhiheng Xu[4,11,17], Peng Jin[3,17], Hongjun Song[1,2,9,12–15,17], Guo-li Ming[1,2,9,12–14,16,17] & Gabsang Lee[1,2,9,12,17]

Zika virus (ZIKV) infection is associated with neurological disorders of both the CNS and peripheral nervous systems (PNS), yet few studies have directly examined PNS infection. Here we show that intraperitoneally or intraventricularly injected ZIKV in the mouse can infect and impact peripheral neurons *in vivo*. Moreover, ZIKV productively infects stem-cell-derived human neural crest cells and peripheral neurons *in vitro*, leading to increased cell death, transcriptional dysregulation and cell-type-specific molecular pathology.

ZIKV, a flavivirus transmitted primarily by *Aedes* mosquitoes, has spread to a growing number of countries. While most ZIKV-infected patients exhibit few or relatively mild symptoms, including mild fever, skin rash, conjunctivitis, muscle and joint pain, malaise or headache, prenatal ZIKV infection may cause microcephaly and other serious brain anomalies in fetuses or infants[1,2]. Recent studies of ZIKV pathogenesis in the CNS have shown that ZIKV crosses the placenta and causes microcephaly by targeting cortical neural progenitor cells, inducing cell death and impairing neurodevelopment[3–8]. Other pronounced symptoms of ZIKV infection in children and adults are retro-orbital pain, abdominal pain and diarrhea[9], which are associated with the PNS, and more specifically sensory and enteric neurons. In particular, peripheral neuropathy without any CNS symptom in a patient infected with ZIKV has been reported[10,11], which is supported by persistent ZIKV detection in the PNS of rhesus macaques[12]. In addition, ZIKV causes Guillain-Barré syndrome (GBS)[1], another PNS disorder. In contrast to CNS model systems[3–6], PNS model systems for investigating ZIKV pathology are limited.

In this study, we investigated PNS infection of ZIKV using both *in vivo* and *in vitro* model systems.

We adopted type-I interferon receptor–deficient (A129) mice to generate a ZIKV infection model *in vivo*. ZIKV SZ01 was injected intraperitoneally into 5-week-old A129 mice, which were inspected 3 d later. To determine the potential for ZIKV infection in the PNS, we examined the dorsal root ganglia (DRG) and small intestine from ZIKV-infected and mock-treated mice. We detected the presence of ZIKV in both DRG and small intestine with ZIKV antiserum (**Supplementary Fig. 1a,b**). In addition, robust ZIKV signals colocalized with neuron-specific class III β-tubulin (Tuj1), indicating that mouse peripheral neurons in the DRG and gut were infected by ZIKV (**Supplementary Fig. 1a,b**). To test whether PNS infection of ZIKV could also occur in a mouse model of microcephaly[5], we injected ZIKV SZ01 into the lateral ventricle of wild-type mouse brains at embryonic day (E) 13.5 and analyzed tissue at postnatal day (P) 1. We also detected ZIKV in the DRG, small intestine and spinal cord, with colocalization with neuronal markers Tuj1 and NeuN or cleaved caspase 3 (cl-Casp3; **Fig. 1** and **Supplementary Fig. 1c,d**), demonstrating that brain-injected ZIKV can infect and impact peripheral neurons in the mouse DRG and gut *in vivo*.

These *in vivo* observations prompted us to use a human stem-cell-based model to directly examine ZIKV infection and its molecular pathology. Neural crest cells are migratory multipotent progenitors that give rise to various cell types, including neurons and glia of the PNS[13]. We previously developed an efficient protocol[14] to differentiate human pluripotent stem cells (hPSCs) into human neural crest cells (hNCCs), which can be further differentiated into human peripheral neurons (hPNs) (**Supplementary Fig. 2**). We used a clinically isolated ZIKV strain from the 2015 Puerto Rico Zika outbreak, PRVABC59 (hereafter ZIKV[PR]), which is closely related to epidemic strains circulating in the Americas that have been linked to *in utero* ZIKV infection[15]. We performed infections at a low or moderate multiplicity of infection (MOI; 0.04 or 0.4) for 2 h. Infection rates were quantified 65 h later with immunocytochemistry using an anti-ZIKV envelope protein (ZIKVE) antibody. hNCCs expressing neural crest markers were readily infected by ZIKV[PR] (**Fig. 2a,b**). As in previous CNS model systems for ZIKV infection[3,16], the staining signal for ZIKVE was concentrated in the perinuclear structures of hNCCs (**Fig. 2a**), and ZIKV[PR] infection reduced the cell viability of hNCCs compared to mock-infected cells (**Fig. 2c** and **Supplementary Fig. 3a**). These results are in accordance with a recent publication demonstrating that ZIKV infects cranial NCCs, resulting in reduced viability[17].

[1]Institute for Cell Engineering, Johns Hopkins University School of Medicine, Baltimore, Maryland, USA. [2]Adrienne Helis Malvin Medical Research Foundation, New Orleans, Louisiana, USA. [3]Department of Human Genetics, Emory University School of Medicine, Atlanta, Georgia, USA. [4]State Key Laboratory of Molecular Developmental Biology, CAS Center for Excellence in Brain Science and Intelligence Technology, Institute of Genetics and Developmental Biology, Chinese Academy of Sciences, Beijing, China. [5]Department of Biological Science, Florida State University, Tallahassee, Florida, USA. [6]Department of Mathematics and Computer Science, Emory University, Atlanta, Georgia, USA. [7]Department of Biostatistics and Bioinformatics, Emory University Rollins School of Public Health, Atlanta, Georgia, USA. [8]Department of Virology, State Key Laboratory of Pathogen and Biosecurity, Beijing Institute of Microbiology and Epidemiology, Beijing, China. [9]Department of Neurology, Johns Hopkins University School of Medicine, Baltimore, Maryland, USA. [10]Departments of Psychiatry and Behavioral Sciences, Cell Biology and Neurology, Emory University School of Medicine, Atlanta, Georgia, USA. [11]Parkinson's Disease Center, Beijing Institute for Brain Disorders, Beijing, China. [12]The Solomon H. Snyder Department of Neuroscience, Johns Hopkins University School of Medicine, Baltimore, Maryland, USA. [13]Department of Neuroscience, and Mahoney Institute for Neurosciences, Perelman School for Medicine, University of Pennsylvania, Philadelphia, Pennsylvania, USA. [14]Institute for Regenerative Medicine, Perelman School for Medicine, University of Pennsylvania, Philadelphia, Pennsylvania, USA. [15]The Epigenetics Institute, Perelman School for Medicine, University of Pennsylvania, Philadelphia, Pennsylvania, USA. [16]Department of Psychiatry and Behavioral Science, Johns Hopkins University School of Medicine, Baltimore, Maryland, USA. [17]These authors jointly directed this work. Correspondence should be addressed to G.-l.M. (gming@mail.med.upenn.edu), H.T. (tang@bio.fsu.edu), Z.X. (zhxu@genetics.ac.cn) or P.J. (peng.jin@emory.edu).
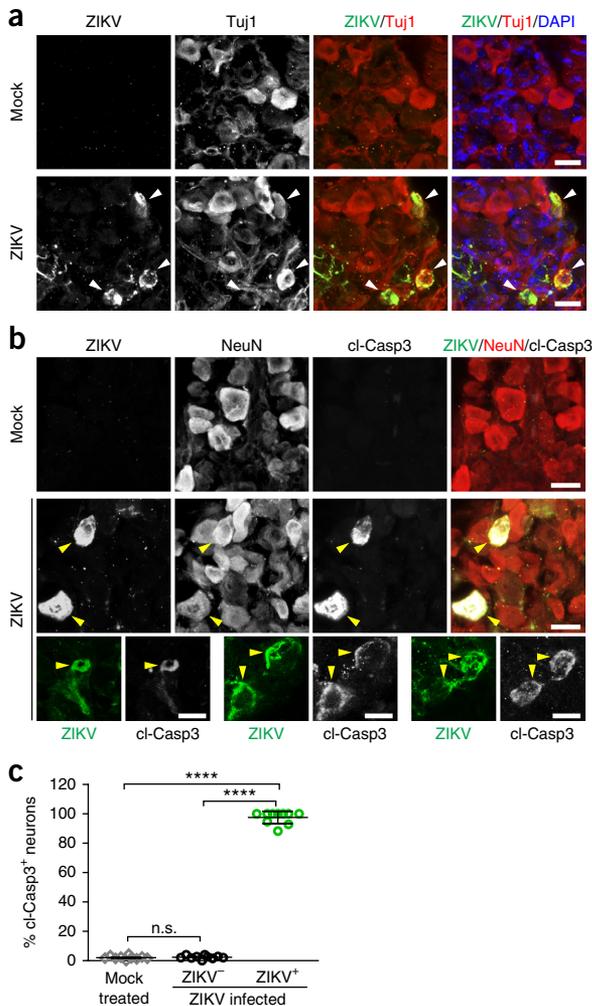
Figure 1 ZIKV infection results in apoptosis of somatosensory neurons in mouse PNS. Mouse embryos were infected by intraventricular injection of 650 plaque-forming units of ZIKV[SZ01] or mock injection at E13.5 and analyzed at P1. (**a**) Representative images of mouse DRG sections stained with the indicated antibodies. White arrowheads, ZIKV-infected DRG neurons. (**b**) Sample images of DRG sections stained with the indicated antibodies. Cleaved caspase 3, cl-Casp3. Yellow arrowheads, ZIKV-infected apoptotic DRG neurons. Scale bars, 20 μm (**a**,**b**). (**c**) The percentage of apoptotic neurons in the mock-treated and ZIKV-infected DRGs. Error bars represent mean ± s.e.m. ****$P < 0.0001$; n.s., not significant; unpaired Student's t-test; $n = 10$ DRGs from 4 pups for each group.

To investigate the impact of ZIKV[PR] infection on hNCCs at the molecular level, we employed global transcriptome analyses (RNA-seq). Our genome-wide analyses identified a large number of genes differentially expressed upon viral infection (**Supplementary Fig. 4a**,**b** and **Supplementary Table 1**). Gene ontology (GO) analyses of ZIKV[PR]-infected hNCCs revealed a particular enrichment of upregulated genes in apoptotic, cell-death-related terms, which was more pronounced than in infected CNS human neural progenitor cells (hNPCs)[3,16], and enrichment in translation-related terms (**Fig. 2d**). The downregulated genes were enriched in cell-cycle-related terms (**Fig. 2e**), which is consistent with our previous findings in CNS hNPCs[3,16]. Transcriptome-wide comparison of gene expression to ZIKV[PR]-infected CNS hNPCs revealed some similarities and differences (**Fig. 2f–i**, **Supplementary Fig. 5** and **Supplementary Table 2**). Between ZIKV[PR]-infected hNCCs and CNS hNPCs, a number of genes were up- and downregulated in common (462 and 643 genes,

respectively), but there were still many genes that were differentially expressed (874 genes in hNCCs and 5,116 genes in CNS hNPCs; **Fig. 2f**,**g** and **Supplementary Fig. 5**). Further GO analyses showed that genes in the term "translational elongation" were uniquely upregulated in ZIKV[PR]-infected hNCCs (false discovery rate (FDR) = 8.4×10^{-39}; **Fig. 2h** and **Supplementary Fig. 5b**) and genes in the term "nucleosome organization" were uniquely downregulated in ZIKV[PR]-infected hNCCs compared to CNS hNPCs (FDR = 3.9×10^{-8}; **Fig. 2i** and **Supplementary Fig. 5b**). This suggests that molecular pathology in ZIKV[PR]-infected hNCCs is distinct from that in CNS hNPCs.

Several recent studies have shown that in the CNS ZIKV targets NPCs, with little direct infection of neurons, both in culture and *in vivo*[3–5,18–20]. In contrast, ZIKV[PR] readily infected hPNs expressing the neuronal markers peripherin (PRPH) and TUJ1 (**Fig. 3a**,**b**). ZIKVE was concentrated in perinuclear structures of the hPSC-derived hPNs (**Fig. 3a**), in accordance with a recent report that infectious ZIKV particles are located in the disrupted endoplasmic reticulum of CNS neurons in the human fetal brain[1]. ZIKV[PR] infection in hPNs led to reduced cell numbers compared to those in mock-infected cells (**Fig. 3c** and **Supplementary Fig. 3b**). Mechanistically, ZIKV[PR] infection increased CASP3 activation in hNCCs and hPNs 65 h after infection, as compared to mock infection, suggesting increased cell death (**Supplementary Fig. 3c–f**). Genome-wide transcription analyses of ZIKV[PR]-infected hPNs identified many differentially expressed genes upon viral infection (**Supplementary Fig. 4c**,**d** and **Supplementary Table 3**). GO analyses of ZIKV[PR]-infected hPNs revealed that differential gene expression patterns were similar to that of ZIKV[PR]-infected hNCCs (**Figs. 2d**,**e** and **3d**,**e**), mainly associated with apoptotic cell death and cell cycle. In ZIKV[PR]-infected hPNs and hNCCs, large numbers of transcripts were differentially expressed (1,983 genes in hPNs and 945 genes in hNCCs), while a subset of these genes were up- and downregulated in common (419 and 615 genes, respectively; **Supplementary Figs. 6** and **7**). Further GO analyses with the list of differentially expressed genes unique to ZIKV[PR]-infected hPNs showed several enriched terms for downregulated genes, including "regulation of cell development" and "regulation of neurogenesis" (**Supplementary Figs. 6g** and **7a**), suggesting that ZIKV[PR] causes substantial developmental and cellular changes in hPNs. In particular, ZIKV[PR] disrupted "WNT signaling pathway" genes in infected hPNs (**Supplementary Fig. 7b**), highlighting marked molecular perturbations upon ZIKV[PR] infection.

To verify our RNA-seq results, we focused on genes associated with apoptosis and epigenetic regulation, using quantitative real-time reverse transcription PCR (qRT-PCR), western blotting and immunocytochemical analyses (**Supplementary Fig. 8**). We confirmed that the expression and phosphorylation levels of c-Jun were increased only in ZIKV[PR]-infected hPNs (**Supplementary Fig. 8c**,**e**,**f**,**i**,**j**), suggesting that c-Jun phosphorylation-associated apoptosis is one of the possible cell death pathways in ZIKV[PR]-infected hPNs (**Supplementary Fig. 9**). We also confirmed that the expression and acetylation levels of histone H3 were decreased only in ZIKV[PR]-infected hNCCs (**Supplementary Fig. 8d**,**g**,**h**), indicating that dysregulation of histone protein expression and acetylation may be associated with cell death of ZIKV[PR]-infected hNCCs (**Supplementary Fig. 9**). Overall, our unbiased global transcriptome data sets not only support our findings of massive cell death in infected hNCCs and hPNs, but also provide a resource to the field for cell-type-specific molecular pathology caused by ZIKV[PR].

While it has been established that ZIKV can cause neural developmental defects during brain development[6], whether ZIKV can efficiently infect hPNs was not previously known. Here we demonstrated that either intraperitoneal injection or fetal mouse brain injection of ZIKV led to infection of the PNS. Both human stem-cell-derived hNCCs and hPNs were permissive to ZIKV infection, presenting far more cell death than

CNS cells. In addition, we found ZIKV infection in human stem-cell-derived Schwann cells, but not in skeletal muscle cells (**Supplementary Fig. 10**), which suggests a tissue-specific vulnerability to ZIKV infection. Our results are also supported by recent human case studies and a primate model study that showed PNS ZIKV pathology[10–12]. We were also able

to detect high levels of ZIKV in mouse spinal cord after intraventricular injection and secretion of infectious ZIKV particles from infected hNCCs and hPNs in culture (**Supplementary Fig. 11**). It remains to be determined how ZIKV can be transmitted from the abdominal cavity or the brain to PNS regions. Potential routes include bloodstream, cerebrospinal
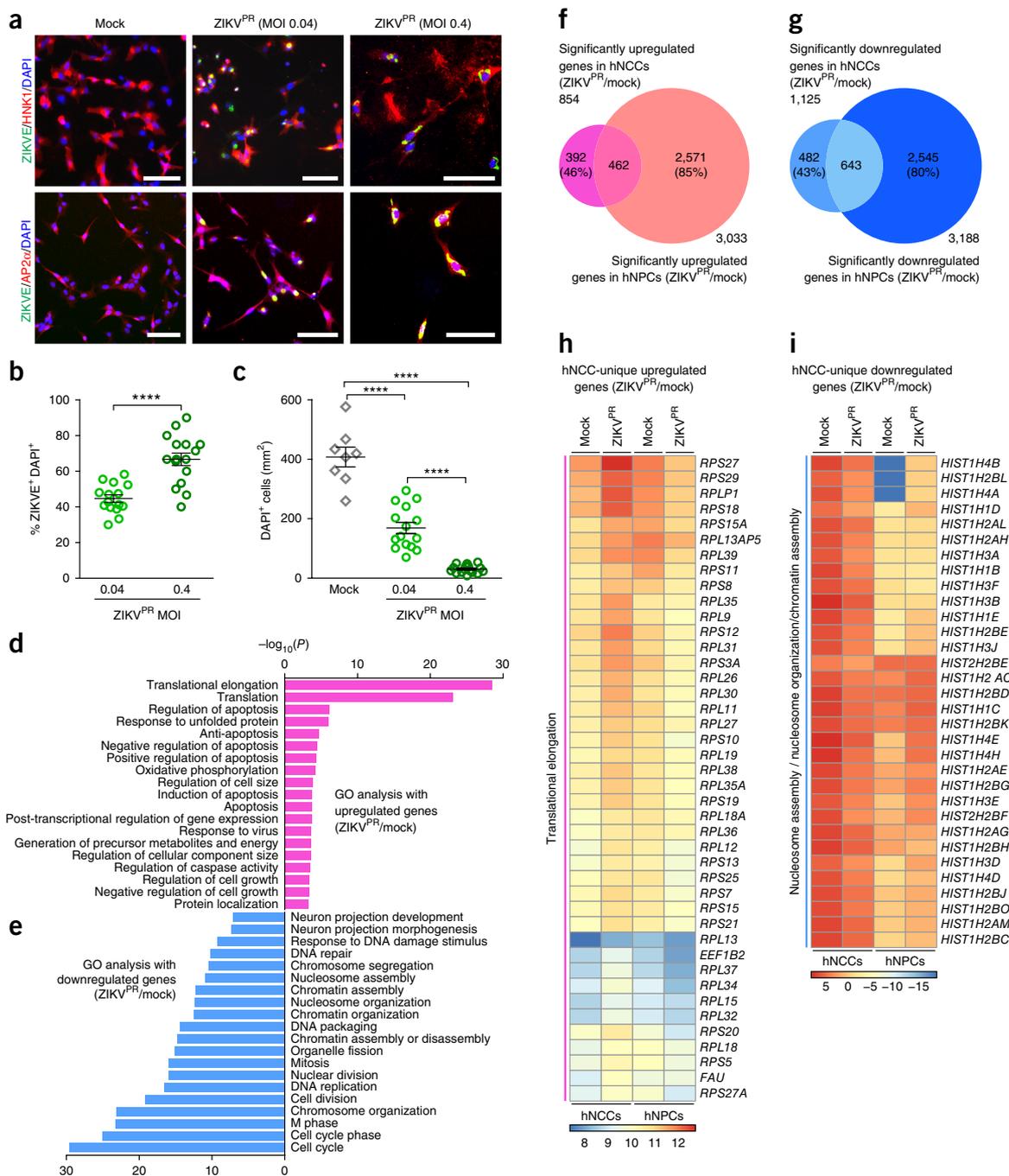
Figure 2 ZIKV efficiently infects human pluripotent stem cell–derived neural crest cells. hNCCs were treated with ZIKV[PR] (MOI of 0.04 or 0.4) or mock-treated for 65 h. (**a**) Representative images of hNCCs immunostained with the indicated antibodies. Scale bars, 100 μm. (**b**) Quantification of the percentage of ZIKVE+ hNCCs, relative to the number of DAPI+ cells ($n = 15$ cultures for MOI of 0.04, $n = 16$ for MOI of 0.4; ****$P < 0.0001$; unpaired Student's t-test). (**c**) The number of DAPI+ hNCCs per mm^2 ($n = 8$ cultures for mock, $n = 15$ for MOI of 0.04, $n = 16$ for MOI of 0.4; ****$P < 0.0001$; unpaired Student's t-test). All error bars represent mean ± s.e.m. (**d,e**) Genes with significant differential expression between infected and uninfected hNCCs were subjected to GO analyses. (**d**) All significant terms for upregulated genes. (**e**) Top 20 most significant terms for downregulated genes. (**f,g**) Weighted Venn diagrams between ZIKV[PR]-infected hNCCs and CNS hNPCs, showing overlap of (**f**) significantly upregulated genes or (**g**) significantly downregulated genes. (**h,i**) Heat maps showing expression levels, in log$_2$(fragments per kilobase of transcript per million mapped reads), of specific genes in mock-infected and ZIKV[PR]-infected hNCCs and hNPCs.
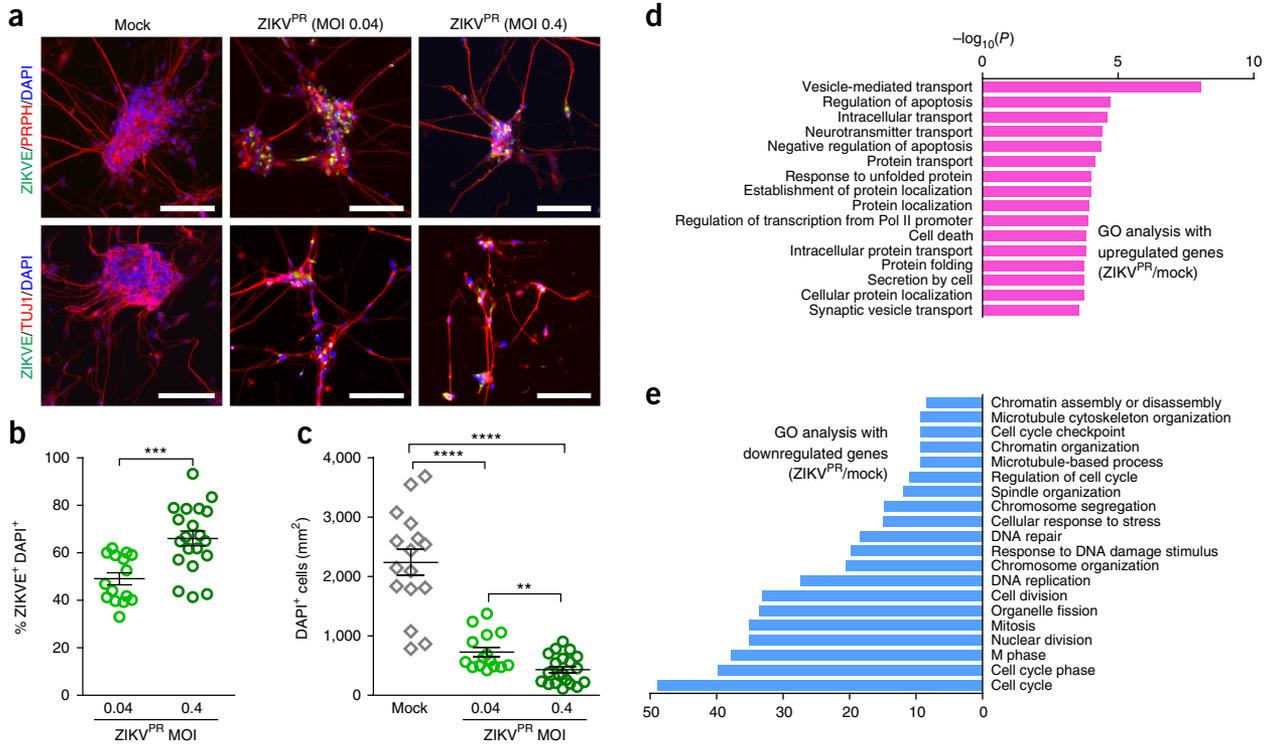
Figure 3 Effective ZIKV infection in human peripheral neurons causes substantial cell death and pathogenic transcriptional dysregulation. hPNs were treated with ZIKV^{PR} (MOI of 0.04 or 0.4) or mock-treated for 65 h. (**a**) Representative images of hPNs immunostained with the indicated antibodies. Scale bars, 100 μm. (**b**) Quantification of the percentage of ZIKVE$^+$ hPNs, relative to the number of DAPI$^+$ cells ($n = 15$ cultures for MOI of 0.04, $n = 20$ for MOI of 0.4; ***$P < 0.001$; unpaired Student's t-test). (**c**) The number of DAPI$^+$ hPNs per mm^2 ($n = 16$ cultures for mock, $n = 15$ for MOI of 0.04, $n = 20$ for MOI of 0.4; **$P < 0.01$; ****$P < 0.0001$; unpaired Student's t-test). All error bars represent mean ± s.e.m. (**d,e**) Genes with significant differential expression between infected and uninfected hPNs were subjected to GO analyses. (**d**) All significant terms for upregulated genes. (**e**) Top 20 most significant terms for downregulated genes.

fluid and interneuronal transmission. It is also important to elucidate how PNS ZIKV infection is relevant to peripheral neuropathies.

In summary, our study provides an efficient humanized model to study ZIKV infection in the PNS, showing similarities and differences in the molecular pathophysiology of ZIKV in the PNS compared to the developing CNS. Our study opens new avenues for further investigating cellular and molecular mechanisms, and our humanized peripheral neuron model can facilitate the discovery and validation of therapeutic agents for ZIKV-related PNS symptoms.

METHODS
Methods, including statements of data availability and any associated accession codes and references, are available in the online version of the paper.

Note: Any Supplementary Information and Source Data files are available in the online version of the paper.

AUTHOR CONTRIBUTIONS
Y.O.: conception and study design, performing experiments, data analysis, data assembly, interpretation of data and writing manuscript; F.Z., Y.W., E.M.L., Q.-F.W., I.Y.C., H.L., F.M., R.L., L.H., T.X., C.L., Z.W. and C.-F.Q.: performing experiments and/or data analysis; H.W., H.T., Z.X., P.J., H.S., G.-l.M. and G.L.: study design and data analysis; H.T., Z.X., P.J., H.S., G.-l.M. and G.L.: conception and study design, data analysis and interpretation, and writing manuscript.

1. Mlakar, J. *et al. N. Engl. J. Med.* **374**, 951–958 (2016).
2. Rasmussen, S.A., Jamieson, D.J., Honein, M.A. & Petersen, L.R. *N. Engl. J. Med.* **374**, 1981–1987 (2016).
3. Tang, H. *et al. Cell Stem Cell* **18**, 587–590 (2016).
4. Cugola, F.R. *et al. Nature* **534**, 267–271 (2016).
5. Li, C. *et al. Cell Stem Cell* **19**, 120–126 (2016).
6. Ming, G.L., Tang, H. & Song, H. *Cell Stem Cell* **19**, 690–702 (2016).
7. Li, H., Saucedo-Cuevas, L., Shresta, S. & Gleeson, J.G. *Neuron* **92**, 949–958 (2016).
8. Wen, Z., Song, H. & Ming, G.L. *Genes Dev.* **31**, 849–861 (2017).
9. Brasil, P. *et al. PLoS Negl. Trop. Dis.* **10**, e0004636 (2016).
10. Medina, M.T. *et al. J. Neurol. Sci.* **369**, 271–272 (2016).
11. Cleto, T.L., de Araújo, L.F., Capuano, K.G., Rego Ramos, A. & Prata-Barbosa, A. *Pediatr. Neurol.* **65**, e1–e2 (2016).
12. Hirsch, A.J. *et al. PLoS Pathog.* **13**, e1006219 (2017).
13. Fuchs, S. & Sommer, L. *Neurodegener. Dis.* **4**, 6–12 (2007).
14. Lee, G., Chambers, S.M., Tomishima, M.J. & Studer, L. *Nat. Protoc.* **5**, 688–701 (2010).
15. Faria, N.R. *et al. Science* **352**, 345–349 (2016).
16. Zhang, F. *et al. Nucleic Acids Res.* **44**, 8610–8620 (2016).
17. Bayless, N.L., Greenberg, R.S., Swigut, T., Wysocka, J. & Blish, C.A. *Cell Host Microbe* **20**, 423–428 (2016).
18. Qian, X. *et al. Cell* **165**, 1238–1254 (2016).
19. Li, H. *et al. Cell Stem Cell* **19**, 593–598 (2016).
20. Onorati, M. *et al. Cell Rep.* **16**, 2576–2592 (2016).

ONLINE METHODS

ZIKV preparation and animal infection. The Asian lineage ZIKV SZ01 strain (GenBank accession code KU866423) was isolated from a patient who had returned to China from Samoa and was amplified in C6/36 cells[21]. The ZIKV replicated efficiently in C6/36 cells and the viral growth curve was determined by qRT-PCR assay. Type-I interferon receptor–deficient (A129) mice were used to generate a ZIKV intraperitoneal infection model. Around 5×10^5 plaque-forming units (PFU) of ZIKV SZ01 or culture medium was injected intraperitoneally into 5-week-old A129 mice, which were inspected 3 d later. To generate the microcephaly mouse model, we anesthetized pregnant ICR mice at embryonic day 13.5 (E13.5), exposed the uterine horns and injected 1 μL of ZIKV SZ01 (6.5×10^5 PFU/mL) or culture medium (RPMI medium 1640 basic + 2% FBS) into the lateral ventricles of embryos using a calibrated micropipette, as described previously[5]. For each pregnant dam, two-thirds of the embryos received ZIKV infection while the rest were injected with culture medium to provide littermate controls. After virus injection, the embryos were placed back into the abdominal cavity of dams and wound was closed. Tissue was collected and analyzed at P1. All experimental procedures were performed in accordance with protocols approved by the Institutional Animal Care and Use Committee at Beijing Institute of Microbiology and Epidemiology and conducted in a biological safety protection laboratory. The experimenters were blinded to treatment. None of the viable animals were excluded from our analyses.

Immunohistochemistry. The trunk tissues with dorsal root ganglion (DRG) and spinal cord from the infected pups and their littermate controls were collected at P1. The tissues were fixed in 4% paraformaldehyde overnight, dehydrated with 20% sucrose in PBS and embedded in OCT compound for cryostat sectioning. The sections with DRG and spinal cord were immunostained with human convalescent serum from ZIKV-infected patients[5] and commercial primary antibodies (**Supplementary Table 4**). For measuring the percentage of apoptotic DRG neurons labeled by cl-Casp3, we counted 10 tissue slices (30 μm/slice) from 4 pairs of animals under fluorescence microscopy. We did not dissect the DRG out of trunk tissues from P1 mice but directly sectioned the trunk tissue containing spinal cord and DRG. We obtained around 10 slices containing DRG tissues from among more than 30 slices for each group and counted the infected and apoptotic neurons for quantification. Some slices contain more than 150 DRG neurons but others had less than 50 DRG. We counted all slices with DRG neurons. Preparations of enteric ganglia were generated by peeling off the small intestinal villus layer from a freshly dissected segment of the jejunum. The stretched surface along with the attached myenteric plexus were fixed overnight in 4% PFA in PBS. The wholemounts were used for immunofluorescence staining. The experimenters were blinded to treatment. None of the viable animals were excluded from our analyses. We also did not exclude any data points from quantification.

hPSC culture and PNS differentiation. Undifferentiated H9 hESCs (passages 40–50) were cultured on mitotically inactivated mouse embryonic fibroblasts (MEFs, Applied Stem Cell) in hESC medium, consisting of DMEM/F12, 20% knockout serum replacement (KSR), 0.1 mM MEM-NEAA, 2 mM L-glutamine, 55 μM β-mercaptoethanol (Life Technologies) and 10 ng/mL FGF2 (R&D Systems). All cells were maintained at 37 °C and 5% CO_2 in a humidified incubator. For neural differentiation, hESCs were plated at $5–20 \times 10^3$ cells on a confluent layer of irradiated (50 Gy) stromal cells (MS-5) in 60-mm cell culture plates in a medium containing DMEM/F12, 20% KSR, 0.1 mM MEM-NEAA, 2 mM L-glutamine and 55 μM β-mercaptoethanol (KSR medium) as described previously[14,22,23]. After 16 d in KSR medium, cultures were switched to N2 medium[14,22–24]. Medium was changed every 2 d, and growth factors were added as described previously[14,22–24]. Briefly, differentiation was initiated by adding 100 nM LDN193189 (Abcam) and 10 μM SB431542 (Cayman Chemical) in KSR medium. Other small-molecule compounds used in neural induction and differentiation were as follows: 0.2 mM ascorbic acid, 0.2 mM dibutyryl cyclic AMP (Sigma-Aldrich) and 1 μM purmorphamine (PMP, Cayman Chemical). Recombinant growth factors were as follows: 50 ng/ml sonic hedgehog (Shh), 100 ng/ml FGF8 (R&D Systems) and 10 ng/ml BDNF (PeproTech). Rosette structures were harvested mechanically at day 22–28 of differentiation (termed passage 0; P0) and gently replated on 15 μg/ml polyornithine/1 μg/ml laminin/10 ng/ml fibronectin (PO/Lam/FN)-coated culture dishes in N2 medium (termed passage 1; P1). P1 cultures were supplemented with ascorbic acid, PMP, Shh, FGF8 and BDNF. After 6–7 d of P1 culture, cells were mechanically triturated after exposure to Ca^{2+}/Mg^{2+}-free Hanks' balanced salt solution (CMF-HBSS, 20 min at 25 °C) and labeled with antibodies for flow cytometry (**Supplementary Table 4**). FACS sorting (p75+ HNK1+) was performed on a MoFlo (Dako). Sorted cells were plated on culture dishes precoated with PO/Lam/FN ($10–30 \times 10^3$ cells/cm²). hPSC-derived hNCCs were maintained in hNCC medium, consisting of Neurobasal medium supplemented with 2 mM L-glutamine, B-27, N-2 supplements (Life Technologies), 20 ng/ml FGF2 and 20 ng/ml EGF (R&D Systems). For directed differentiation of hPSC-derived NCCs toward hPNs, FGF2/EGF-expanded hNCCs were differentiated for at least for 2 weeks with hPN medium, consisting of Neurobasal medium supplemented with 2 mM L-glutamine, B-27, N-2 supplements, 0.2 mM ascorbic acid, 0.2 mM dibutyryl cyclic AMP, 10 ng/mL BDNF, 10 ng/mL NGF (PeproTech) and 10 ng/mL GDNF (R&D Systems)[23]. For directed differentiation of hPSC-derived NCCs toward Schwann cells, we followed a previously described protocol[14,22]. Myogenic differentiation and myotube formation followed a previously described protocol[25].

hPSC culture and CNS hNPC differentiation. Human iPSC lines have been fully characterized[26] and were passaged on MEF feeder layers. All studies followed institutional IRB and ISCRO guidelines and protocols approved by Johns Hopkins University School of Medicine. Human iPSCs were differentiated into forebrain-specific hNPCs and immature neurons following a previously established protocol[26]. Briefly, hiPSCs colonies were detached from the feeder layer with 1 mg/mL collagenase treatment for 1 h and suspended in embryonic body (EB) medium, consisting of FGF2-free iPSC medium supplemented with 2 μM dorsomorphin and 2 μM A-83, in untreated polystyrene plates for 4 d with daily medium changes. After 4 d, EB medium was replaced by neural induction medium (hNPC medium), consisting of DMEM/F12, N2 supplement, NEAA, 2 μg/mL heparin and 2 μM cyclopamine. The floating EBs were then transferred to Matrigel-coated six-well plates at day 7 to form neural-tube-like rosettes. The attached rosettes were kept for 15 d with hNPC medium changed every other day. On day 22, the rosettes were picked mechanically and transferred to low-attachment plates (Corning) to form neurospheres in hNPC medium containing B27. The neurospheres were then dissociated with Accutase at 37 °C for 10 min and placed onto Matrigel-coated six-well plates at day 24 to form monolayer hNPCs in hNPC medium containing B27. These hNPCs expressed forebrain-specific progenitor markers, including NESTIN, PAX6, EMX-1, FOXG1 and OTX2 (ref. 26).

Preparation of ZIKV^PR and cell infection. The ZIKV PRVABC59 strain (ZIKV^PR) was obtained from ATCC (Manassas, VA) and subsequently amplified in *Aedes albopictus* clone C6/36 cells (ATCC). Briefly, C6/36 cells were inoculated with viral inoculum for 1 h at 28 °C in a low volume of medium (3 mL per T-75 flask), with rocking every 15 min, before the addition of an additional 17 mL medium. Virus-inoculated cells were then incubated at 28 °C for 6–7 d before harvesting the supernatant. C6/36-amplified ZIKV^PR titer was determined by infecting Vero cells for 48 h with a methylcellulose overlay and analyzed for focus-forming units (FFU) per mL. In mock infections, an equal volume of spent uninfected C6/36 culture medium was used. hPSC-derived hNCCs were seeded at a density of 50 cells/mm² and maintained for 2–4 d before ZIKV infection. hNCC-derived hPNs were seeded at a density of 1,700 cells/mm² and matured for 2–3 weeks before ZIKV infection. Then these cells were infected with ZIKV^PR at MOI of 0.04 or 0.4 and analyzed 65 h after infection after washing the cells three times with culture medium or PBS. The experimenter was not blinded to treatment. None of cell cultures were excluded from our analyses.

Immunocytochemistry. Cells were fixed in 4% paraformaldehyde and stained with primary antibodies (**Supplementary Table 4**) after permeabilization with 0.1% Triton X-100/0.5% BSA/PBS solution. Appropriate Alexa Fluor 488- or 568-labeled secondary antibody (Life Technologies) and DAPI (Roche Applied Science) nuclear counter-staining were used for visualization. The stained samples were analyzed using fluorescence microscopy (Eclipse TE2000-E, Nikon). The numbers of ZIKVE+, Ki-67+ or DAPI+ cells per mm² were counted under fluorescence microscopy. Cell viability 65 h after ZIKV^PR infection was represented as percentage fold change (relative to mock) of DAPI+ cell number (per mm²) in ZIKV^PR-infected cells (mean ± s.e.m.). The experimenter was not blinded to treatment. None of cell cultures were excluded from our analyses.

RNA isolation, RNA-seq library preparation and sequencing. RNA-seq libraries were prepared from isolated total RNA and were sequenced as previously described[16]. Briefly, total cellular RNA was purified from cell pellets using TRIzol reagent (Life Technologies) according to the manufacturer's instructions. RNA-seq libraries were generated from 1 μg of total RNA from duplicated or triplicated samples (2 or 3 cell cultures) per condition using the TruSeq LT RNA Library Preparation Kit v2 (Illumina) following the manufacturer's protocol. An Agilent 2100 BioAnalyzer and DNA1000 kit (Agilent) were used to quantify amplified cDNA and to control the quality of the libraries. An Illumina HiSeq2500 or HiSeq3000 was used to perform 100- or 50-cycle single-read sequencing. Image processing and sequence extraction were performed using the standard cloud-based Illumina pipeline in BaseSpace. The experimenter was blinded to treatment.

Bioinformatic analyses. Single-end RNA-seq reads were first aligned to human transcriptome annotations and genome assembly (hg19) using TopHat[27] v2.0.13. The numbers of mapped reads for each condition can be found in **Supplementary Tables 1** and **3**. FPKM (fragments per kilobase of transcript per million mapped reads) values were calculated by Cufflinks[28] v2.2.1. Pairwise comparisons between infected and mock conditions were performed to detect differentially expressed (DE) genes using Cuffdiff[28] v2.2.1. In hPNs and hNCCs, DE genes are defined as ones with q less than 0.05; and in CNS hNPCs, DE genes are defined as ones with q less than 0.05 and absolute $\log_2$ fold change of expression no less than 0.57 (the same significance cut-off used by Cuffdiff for the RNA-seq data of hNCCs). Gene ontology (GO) analyses on biological processes were performed by the Database for Annotation, Visualization and Integrated Discovery (DAVID)[29] v6.7. To identify significantly enriched GO terms, a Benjamini–Hochberg procedure was used to control the false discovery rate (FDR) at 0.05. Pathway enrichment analyses and disease-related gene enrichment analyses were performed by the web-based Gene SeT AnaLysis Toolkit (WebGestalt)[30] update 2015 with adjusted P no greater than 0.05. The experimenter was blinded to treatment.

qRT-PCR. Total RNA was extracted by using the TRIzol Reagent and reverse transcribed by using High Capacity cDNA Reverse Transcription Kit (Applied Biosystems). qRT-PCR mixtures were prepared with KAPA SYBR FAST qPCR Kit Master Mix (Kapa Biosystems) and reactions were done with the Mastercycler ep Realplex2 (Eppendorf). Each transcript level was assessed by qRT-PCR normalized to *GAPDH* expression. Primers for qRT-PCR are listed in **Supplementary Table 5**. The experimenter was not blinded to treatment. None of cell cultures were excluded from our analyses.

Western blot analyses. Cells were lysed in RIPA buffer (Cell Signaling Technology) and supplemented with 1% SDS, 10% glycerol and 1 mM PMSF. After sonicating to reduce the viscosity, cell lysates were mixed with Benzonase (Sigma-Aldrich) and incubated for 15 min at 37 °C. The samples were clarified by centrifugation at 15,000*g* for 30 min at 14 °C, boiled at 98 °C for 2 min in Laemmli sample buffer (Sigma-Aldrich) supplemented with 20 mM DTT, resolved by SDS-PAGE and transferred to nitrocellulose membranes (Bio-Rad). Western blot analyses were performed with the indicated antibodies (**Supplementary Table 4**). The bands were quantified by densitometry using ImageJ (NIH). The experimenter was not blinded to treatment. Uncropped blots are shown in **Supplementary Figure 12**.

Viral titer by focus forming assay. Cells were infected with ZIKV[PR] at MOI of 0.04 for 65 h before harvesting the supernatant. Human cell amplified ZIKV[PR] titer was determined by infecting Vero cells for 48 h with a methylcellulose overlay and analyzed for FFUs per mL as previously described[31]. The experimenter was not blinded to treatment.

Statistical analysis. All data were tested for normal distribution. Values are from at least three independent experiments with multiple biological replicates each and reported as mean ± s.e.m. Differences between two samples were analyzed for significance using the unpaired two-tailed Student's *t*-test in Prism (GraphPad). No statistical methods were used to predetermine sample sizes, but our sample sizes are similar to those reported in previous publications[3,5,16,18,22,23,26,31]. Experimenters using *in vivo* samples were always blinded to treatment. No special randomization procedures were used for assigning groups.

A **Life Sciences Reporting Summary** is available.

Code availability. TopHat[27] v2.0.13 and Cuffdiff[28] v2.2.1, used for data analysis, are freely available at https://ccb.jhu.edu/software/tophat/index.shtml and http://cole-trapnell-lab.github.io/cufflinks/cuffdiff/. R packages ggplot2 and pheatmap used for data visualization are freely available at http://ggplot2.org/ and the Comprehensive R Archive Network (CRAN).

Data availability. The RNA-seq data reported in this paper has been deposited in GEO, GSE87750. The remaining data that support the findings of this study are available from the corresponding authors upon reasonable request.

21. Deng, Y.Q. *et al. Sci. China Life Sci.* **59**, 428–430 (2016).
22. Lee, G. *et al. Nat. Biotechnol.* **25**, 1468–1475 (2007).
23. Oh, Y. *et al. Cell Stem Cell* **19**, 95–106 (2016).
24. Perrier, A.L. *et al. Proc. Natl. Acad. Sci. USA* **101**, 12543–12548 (2004).
25. Choi, I.Y. *et al. Cell Rep.* **15**, 2301–2312 (2016).
26. Wen, Z. *et al. Nature* **515**, 414–418 (2014).
27. Kim, D. *et al. Genome Biol.* **14**, R36 (2013).
28. Trapnell, C. *et al. Nat. Biotechnol.* **31**, 46–53 (2013).
29. Huang, W., Sherman, B.T. & Lempicki, R.A. *Nat. Protoc.* **4**, 44–57 (2009).
30. Wang, J., Duncan, D., Shi, Z. & Zhang, B. *Nucleic Acids Res.* **41**, W77–W83 (2013).
31. Xu, M. *et al. Nat. Med.* **22**, 1101–1107 (2016).

naturereserach

Corresponding author(s):   Guo-li Ming

☐ Initial submission   ☐ Revised version   ☒ Final submission

Life Sciences Reporting Summary

Nature Research wishes to improve the reproducibility of the work that we publish. This form is intended for publication with all accepted life science papers and provides structure for consistency and transparency in reporting. Every life science submission will use this form; some list items might not apply to an individual manuscript, but all fields must be completed for clarity.

For further information on the points included in this form, see Reporting Life Sciences Research. For further information on Nature Research policies, including our data availability policy, see Authors & Referees and the Editorial Policy Checklist.

▶ Experimental design

1. Sample size

Describe how sample size was determined.

Although pre-study sample size calculations were not made, the majority of experiments in vitro were performed using multiple batches of differentiation, and multiple technical repeats to ensure robustness. All the sample sizes in each panel/graph are provided in the Figure Legends. For in vivo experiments, we collected DRG tissues from 4 control and 4 ZIKV-infected mice. For each animals, we examined at least 5 DRGs wherein there were more than 100 DRG neurons. There were striking ZIKV infection in the spinal cord of all 4 animals. Sample size was adequate due to binary nature of the reported phenomenon (either present or absent).

2. Data exclusions

Describe any data exclusions.

None of the viable animals or cell cultures were excluded from our analyses. We also did not exclude any data points for quantification.

3. Replication

Describe whether the experimental findings were reliably reproduced.

All attempts at replication were successful.

4. Randomization

Describe how samples/organisms/participants were allocated into experimental groups.

Whereas randomization was not feasible for in vitro study, batch effects were minimized through simultaneous processing of cases and controls for all experiments. For the ZIKV infection in the juvenile type-I interferon receptor deficient (A129) mice, we randomly grouped the animals and performed the ZIKV injection. To induce ZIKV-infection in the embryonic brains, we randomly selected two thirds of embryos for intraventricular ZIKV injection. After the birth of pups, we collected tissues from all of the viable mice without prior knowledge of whether the individual pups were ZIKV-infected or not. The identification completely relied on immunostaining with human ZIKV antibodies.

5. Blinding

Describe whether the investigators were blinded to group allocation during data collection and/or analysis.

Blinding was not utilized in vitro study. As primarily molecular techniques were utilized, investigator bias should play a minimal role in data acquisition in this particular study. For the embryonic infection model, we performed the experiment blindly. When we collected the DRG tissues from pups, we had no prior knowledge of which animals were infected with ZIKV. The samples were identified to be ZIKV-positive or negative by researchers in Dr. Zhiheng Xu's lab. The subsequent staining with cell markers and apoptotic marker were mainly performed in Dr. Qing-Feng Wu's lab.

Note: all studies involving animals and/or human research participants must disclose whether blinding and randomization were used.

6. Statistical parameters

For all figures and tables that use statistical methods, confirm that the following items are present in relevant figure legends (or in the Methods section if additional space is needed).

n/a	Confirmed	
☐	☒	The <u>exact sample size</u> (*n*) for each experimental group/condition, given as a discrete number and unit of measurement (animals, litters, cultures, etc.)
☐	☒	A description of how samples were collected, noting whether measurements were taken from distinct samples or whether the same sample was measured repeatedly
☐	☒	A statement indicating how many times each experiment was replicated
☐	☒	The statistical test(s) used and whether they are one- or two-sided (note: only common tests should be described solely by name; more complex techniques should be described in the Methods section)
☐	☒	A description of any assumptions or corrections, such as an adjustment for multiple comparisons
☐	☒	The test results (e.g. *P* values) given as exact values whenever possible and with confidence intervals noted
☐	☒	A clear description of statistics including <u>central tendency</u> (e.g. median, mean) and <u>variation</u> (e.g. standard deviation, interquartile range)
☐	☒	Clearly defined error bars

See the web collection on statistics for biologists for further resources and guidance.

▶ Software

Policy information about availability of computer code

7. Software

Describe the software used to analyze the data in this study.	TopHat v2.0.13 (ref, Kim, D. et al. Genome Biol. 14, R36 (2013)) and Cuffdiff v2.2.1 (ref, Trapnell, C. et al. Nat. Biotechnol. 31, 46-53 (2013)) used for data analysis are freely available at https://ccb.jhu.edu/software/tophat/index.shtml and http://cole-trapnell-lab.github.io/cufflinks/cuffdiff/. R packages ggplot2 and pheatmap used for data visualization are freely available at http://ggplot2.org/ and the Comprehensive R Archive Network (CRAN).

For manuscripts utilizing custom algorithms or software that are central to the paper but not yet described in the published literature, software must be made available to editors and reviewers upon request. We strongly encourage code deposition in a community repository (e.g. GitHub). *Nature Methods* guidance for providing algorithms and software for publication provides further information on this topic.

▶ Materials and reagents

Policy information about availability of materials

8. Materials availability

Indicate whether there are restrictions on availability of unique materials or if these materials are only available for distribution by a for-profit company.	No unique materials were used.

9. Antibodies

Describe the antibodies used and how they were validated for use in the system under study (i.e. assay and species).	All antibodies were validated by the manufacturer and/or by our previous publications (Tang, H. et al. Cell Stem Cell 18, 587-590 (2016); Li, C. et al. Cell Stem Cell 19, 120-126 (2016); Lee, G. et al. Nat. Biotechnol. 25, 1468-1475 (2007); Lee, G. et al. Nat. Protoc. 5, 688-701 (2010); Oh, Y. et al. Cell Stem Cell 19, 95-106 (2016)).

10. Eukaryotic cell lines

a. State the source of each eukaryotic cell line used.	Undifferentiated H9 hESCs are purchased from WiCell.
b. Describe the method of cell line authentication used.	None of the cell lines used have been authenticated.
c. Report whether the cell lines were tested for mycoplasma contamination.	We have tested for mycoplasma contamination every other week and have continuously maintained a mycoplasma free laboratory for over five years.
d. If any of the cell lines used are listed in the database of commonly misidentified cell lines maintained by ICLAC, provide a scientific rationale for their use.	No commonly misidentified cell lines were used.

▶ Animals and human research participants

Policy information about studies involving animals; when reporting animal research, follow the ARRIVE guidelines

11. Description of research animals

Provide details on animals and/or animal-derived materials used in the study.

We provide two ZIKV-infected mouse models in the manuscript. In one of our disease model, the type-I interferon receptor deficient (A129) mice received intraperitoneal injection of ZIKV. Approximately 5× 10 5 plaque-forming unit (PFU) of ZIKV SZ01 was applied to 5-week-old A129 mice which were examined 3 days post injection. For the other mouse model, the pregnant ICR mice (n = 3) were anesthetized at embryonic day 13.5 and injected with 1μL of ZIKV SZ01 (6.5×10 5 PFU/mL) or culture medium as mock into the lateral ventricles of embryos using a calibrated micropipette. For each pregnant dam, two thirds of the embryos received ZIKV infection while the rest were injected with culture medium to provide littermate controls. After virus injection, the embryos were placed back into the abdominal cavity of dams and wound was closed. The dorsal root ganglion (DRG) and spinal cord (SC) tissues were harvested and analyzed at postnatal day 1. All experimental procedures were performed in accordance with protocols approved by the Institutional Animal Care and Use Committee at Beijing Institute of Microbiology and Epidemiology and conducted in a biological safety protection laboratory.

Policy information about studies involving human research participants

12. Description of human research participants

Describe the covariate-relevant population characteristics of the human research participants.

This study did not involve human research participants.